

# ChemComm

Chemical Communications

Accepted Manuscript

This article can be cited before page numbers have been issued, to do this please use: X. Xin, S. Du, Y. Xiao, H. Zou, Y. Bao, Y. Qi, S. Jin, Z. Feng and F. Zhang, *Chem. Commun.*, 2025, DOI: 10.1039/D5CC04308E.



This is an Accepted Manuscript, which has been through the Royal Society of Chemistry peer review process and has been accepted for publication.

Accepted Manuscripts are published online shortly after acceptance, before technical editing, formatting and proof reading. Using this free service, authors can make their results available to the community, in citable form, before we publish the edited article. We will replace this Accepted Manuscript with the edited and formatted Advance Article as soon as it is available.

You can find more information about Accepted Manuscripts in the [Information for Authors](#).

Please note that technical editing may introduce minor changes to the text and/or graphics, which may alter content. The journal's standard [Terms & Conditions](#) and the [Ethical guidelines](#) still apply. In no event shall the Royal Society of Chemistry be held responsible for any errors or omissions in this Accepted Manuscript or any consequences arising from the use of any information it contains.

## COMMUNICATION

Facet-dependent spatial charge separation in metals-doped SrTiO<sub>3</sub> photocatalyst with visible light utilizationXueshang Xin,<sup>ab</sup> Shiwen Du,<sup>a</sup> Yejun Xiao,<sup>c</sup> Hai Zou,<sup>ab</sup> Yunfeng Bao,<sup>a</sup> Yu Qi,<sup>a</sup> Shengye Jin,<sup>c</sup> Zhaochi Feng,<sup>a</sup> and Fuxiang Zhang<sup>\*a</sup>Received 00th January 20xx,  
Accepted 00th January 20xx

DOI: 10.1039/x0xx00000x

**Visible-light-responsive Rh/Sb co-doped SrTiO<sub>3</sub> with engineered {100}/{110} facets (STO:RS(NaCl)) was synthesized via flux-assisted crystallization. Facet-dependent spatial charge separation, driven by work function differences, enabled electrons and holes to migrate to respective facets. This configuration tripled photocatalytic hydrogen evolution versus non-faceted STO:RS(w/o), overcoming the limitations of ultraviolet-only absorption and inefficient charge separation.**

Solar-driven water splitting using semiconductor photocatalysts offers sustainable energy solutions, yet efficient charge separation remains critical.<sup>1</sup> Rapid carrier recombination severely limits photocatalytic efficiency.<sup>2,3</sup> While cocatalyst deposition enhances carrier extraction,<sup>4</sup> traditional impregnation (imp.) or adsorption methods often yield randomly distributed cocatalysts with proximal redox sites, promoting electron-hole recombination. Controlled synthesis of anisotropic facets addresses this challenge by spatially separating electrons and holes,<sup>5</sup> as demonstrated in TiO<sub>2</sub>, BiVO<sub>4</sub> and others.<sup>6-8</sup> Moreover, selective photodeposition of reduction/oxidation cocatalysts on electron/hole-rich facets further boosts carrier utilization efficiency and photocatalytic activity. Spatial separation of photogenerated carriers between the {100} and {110} facets of BiVO<sub>4</sub> led to a 17-fold enhancement in water oxidation activity after selective cocatalyst deposition.<sup>9</sup> Notably, anisotropic crystal facets exhibit distinct work functions, causing varied surface band bending and driving electron and hole migration in different spatial directions under the influence of the built-in electric

field.<sup>10</sup> However, the synthesis of anisotropic facets remains challenging, limiting availability of photocatalysts with spatial charge separation, especially for metal ion-doped materials.

Since its initial report in 1980, SrTiO<sub>3</sub> (STO) has been extensively studied for photocatalysis.<sup>11</sup> Various strategies have been employed to enhance its photocatalytic performance,<sup>12</sup> including the induction of spatial charge separation through the exposure of anisotropic facets.<sup>13,14</sup> Domen et al. reported Al-modified STO with exposed {100}/{110} facets, which could selectively load dual cocatalysts on different facets, achieving nearly unity quantum efficiency.<sup>10</sup> However, the solar-to-hydrogen (STH) efficiency of STO remains < 1% due to its UV-only response.<sup>15</sup> Doping is a commonly used and effective method to enhance the light-harvesting capacity and enable visible light response by introducing doping energy levels within the bandgap or modifying the valence band maximum (VBM) and conduction band minimum (CBM) positions through orbital hybridization.<sup>16</sup> Yet, controlling facets in metal-doped STO for extended visible-light utilization and their potential spatial charge separation remains understudied.

In this study, visible-light-responsive STO (STO:RS(NaCl)) with {100}/{110} facets was synthesized via Rh/Sb co-doping and NaCl flux treatment. Photodeposition confirmed the occurrence of spatial charge separation, while theoretical calculations revealed that anisotropic facet work function differences drive directional carrier migration. Photoluminescence (PL) and transient absorption spectroscopy (TAS) confirmed that spatial charge separation effectively enhances carrier utilization. Selective photodeposition of reduction/oxidation cocatalysts onto the respective {100}/{110} facets further enhanced carrier extraction and photocatalytic activity.

The synthesis route was schematically depicted in Fig. S1. Under high-temperature conditions in molten NaCl, STO:RS undergoes a continuous dissolution-recrystallization process. Na<sup>+</sup> ions adsorb onto the high-index facets, reducing surface free energy. According to crystal growth principles (Gibbs-Wulff theorem), the growth rate of a crystal facet is proportional to

<sup>a</sup> State Key Laboratory of Catalysis, Dalian National Laboratory for Clean Energy, Dalian Institute of Chemical Physics, Chinese Academy of Sciences, Dalian, 116023, China. E-mail: fxzhang@dicp.ac.cn.

<sup>b</sup> Center of Materials Science and Optoelectronics Engineering, University of Chinese Academy of Sciences, Beijing, 100049, China.

<sup>c</sup> State Key Laboratory of Molecular Reaction Dynamics, Dalian Institute of Chemical Physics, Chinese Academy of Sciences, Dalian, 116023, China.

<sup>†</sup> Electronic supplementary information (ESI) available. See DOI: 10.1039/x0xx00000x



its surface energy. Consequently, the reduction in surface energy dramatically slows the growth kinetics and ultimately leads to the exposure of high-index facets.<sup>17</sup> The scanning electron microscopy (SEM) images showed that the STO:RS precursor particles (< 50 nm, Fig. S2) underwent NaCl-assisted calcination to form faceted STO:RS(NaCl) with {100}/{110} exposure (Fig. 1c), whereas NaCl-free calcination yielded sintered STO:RS(w/o) with irregular morphology (Fig. 1d). Additionally, the high-angle annular dark-field scanning transmission electron microscopy (HAADF-STEM) images (Fig. S3) revealed a smooth surface structure and a highly ordered atomic arrangement from the surface to the bulk, confirming the single-crystalline nature of STO:RS(NaCl). The lattice spacings (0.39 nm and 0.28 nm) on adjacent facets and atomic arrangement directions corroborate that the exposed facets of STO:RS(NaCl) are {100} and {110}.

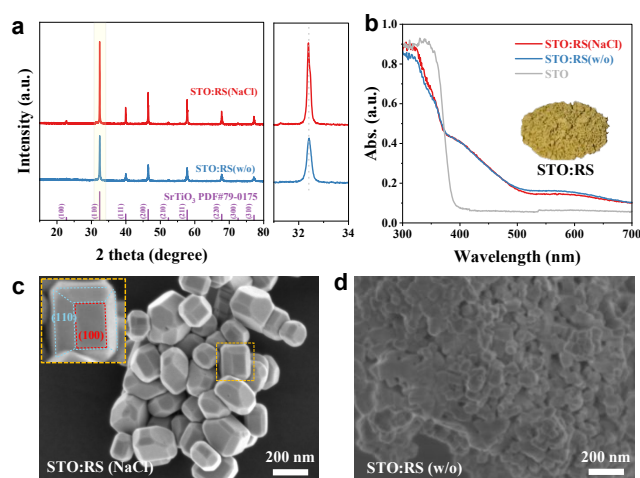


**Fig. 1** (a) XRD patterns, (b) UV-vis DRS, and (c)-(d) SEM images of STO:RS(NaCl) and STO:RS(w/o).

X-ray diffraction (XRD) patterns (Fig. 1a) for both STO:RS(w/o) and STO:RS(NaCl) were in good agreement with the cubic perovskite  $\text{SrTiO}_3$  ( $Pm\bar{3}m$ , JCPDS No. 79-0175). Furthermore, Rietveld refinements were used to analyze the crystal structure of two samples. As shown in Fig. S4 and Table S1, reasonable goodness-of-fit parameters were obtained when Rh, Sb and Ti occupy the same crystallographic positions. According to Vegard's law,<sup>18</sup> the calculated unit cell dimensions of STO:RS(NaCl) and STO:RS(w/o) showed only a limited difference compared to STO. This is attributed to the relative balance achieved by doping large-radius  $\text{Rh}^{3+}$  (0.665 Å) and small-radius  $\text{Sb}^{5+}$  (0.60 Å) ions into the  $\text{Ti}^{4+}$  (0.605 Å) sites.<sup>19</sup> Inductively coupled plasma optical emission spectrometry (ICP-OES) analysis (Table S2) verified that the Rh and Sb concentrations in both STO:RS(NaCl) and STO:RS(w/o) were comparable. X-ray photoelectron spectra (XPS) analysis further demonstrated that the valence states of Rh, Sb and Ti in both samples were nearly the same (Fig. S5). The above results indicated that Rh and Sb were successfully doped into STO:RS(NaCl) and STO:RS(w/o).

UV-vis diffuse reflectance spectra (DRS) revealed visible-light absorption in both STO:RS(NaCl) and STO:RS(w/o) (Fig. 1b), contrasting with UV-only absorption in pristine STO. These absorption bands could respectively be assigned to  $\text{Rh}^{3+} \rightarrow \text{CBM}$

transitions (390-520 nm) and  $\text{VBM} \rightarrow \text{Rh}^{4+}$  transitions ( $\sim 580$  nm). Notably,  $\text{Sb}^{5+}$  does not affect the light absorption of STO, but only reduces the presence of  $\text{Rh}^{4+}$  through charge balance.<sup>20</sup> Density functional theory (DFT) simulations (Fig. S6) revealed that Rh doping introduces new energy levels within the bandgap, while Sb leaves band edges unaffected. Additionally, STO:RS maintains pristine STO's indirect bandgap characteristic. Tauc plots showed comparable bandgaps ( $\sim 2.44$  eV) for both samples (Fig. S7a). Mott-Schottky (MS) analysis (Fig. S7b) revealed a more negative flat-band potential for STO:RS(NaCl) ( $-0.18$  eV vs.  $-0.12$  eV for STO:RS(w/o)), which was attributed to exposed facets differences.<sup>21</sup> The positive curve slope confirms n-type behavior, where CBM is typically 0.1-0.2 eV above the flat-band potential,<sup>22</sup> with bandgaps obtained from Tauc plots, the VBM and CBM were estimated (Fig. S7c).

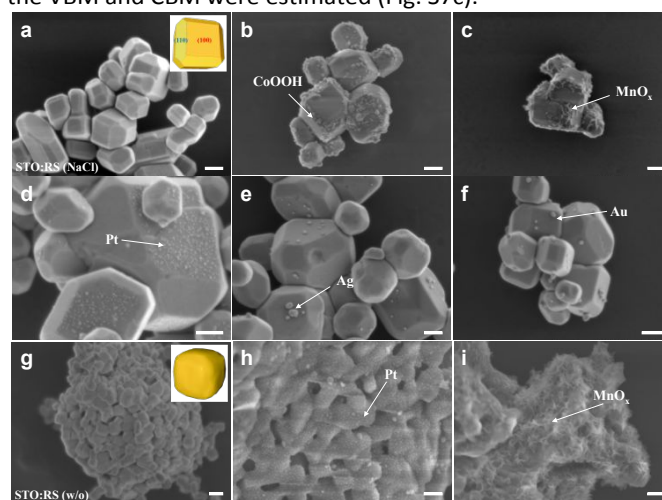


**Fig. 2** SEM images of (a) STO:RS(NaCl) and STO:RS(NaCl) loaded with (b) CoOOH, (c)  $\text{MnO}_x$ , (d) Pt, (e) Ag, (f) Au by photodeposition. SEM images of (g) STO:RS(w/o) and STO:RS(w/o) loaded with (h) Pt, (i)  $\text{MnO}_x$  by photodeposition, the scale is 100 nm.

The facet-dependent spatial charge separation in STO:RS(NaCl) was systematically investigated through redox-selective photodeposition ( $\lambda \geq 420$  nm, Fig. 2a-f). Metal oxides (CoOOH and  $\text{MnO}_x$ ) were preferentially accumulated on {110} facet (hole-rich),<sup>23</sup> while metals (Pt/Ag/Au) were selectively deposited on the {100} facet (electron-rich). Energy dispersive X-ray spectroscopy (EDS) mappings of the Ag/STO:RS(NaCl) and  $\text{MnO}_x$ /STO:RS(NaCl) (Fig. S8) showed that the Ag and  $\text{MnO}_x$  were successfully deposited on the surface, respectively. XPS analysis further confirmed the presence of metals and metal oxides (Fig. S9). According to the binding energy, both Ag and Au were in metallic form, while Co and Mn existed in the form of CoOOH and  $\text{MnO}_x$  ( $1.5 < x < 2$ ). Notably, platinum exhibited incomplete reduction with coexisting metallic Pt and partially reduced Pt(II)O species, which was consistent with previously reported Pt(IV) reduction characteristics.<sup>13</sup> These results directly correlated facet electronic properties with redox selectivity. As a comparison, impregnation-loaded Pt on STO:RS(NaCl) showed random distribution (Fig. S10a), ruling out thermodynamic adsorption preference as the cause of facet selectivity. In addition, Pt showed random deposition



orientation and was independent of the deposition method (Fig. S11), ruling out lattice matching or epitaxial effects. Furthermore, dual  $\text{MnO}_x/\text{Au}$  photodeposition validated charge rectification, with  $\text{MnO}_x$  on {110} and Au on {100} facet, achieving spatial separation of dual species on the surface (Fig. S10b). In contrast, irregular  $\text{STO:RS(w/o)}$  showed random Pt/ $\text{MnO}_x$  distributions (Fig. 2g-i). This contrast stemmed from divergent carrier dynamics: anisotropic facets in  $\text{STO:RS(NaCl)}$  enabled directional transport, whereas disordered  $\text{STO:RS(w/o)}$  permitted random migration.

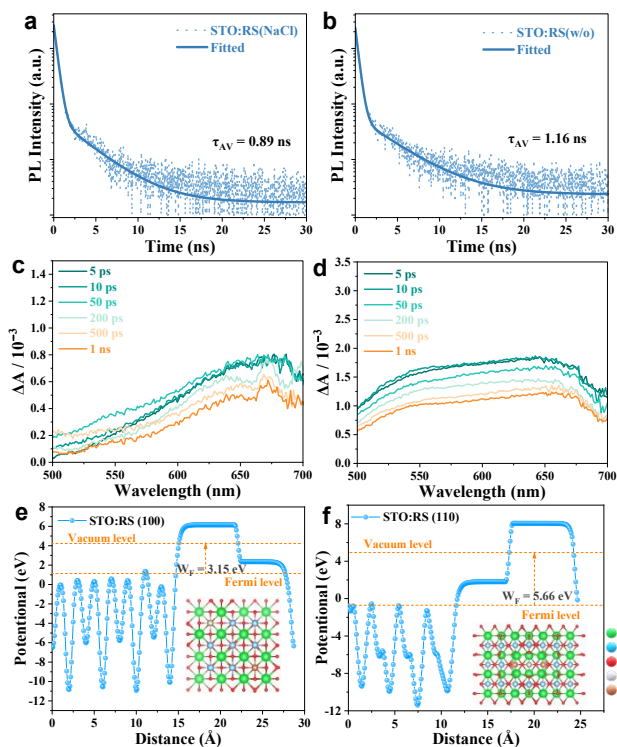


**Fig. 3** TRPL decay curves of (a)  $\text{STO:RS(NaCl)}$  and (b)  $\text{STO:RS(w/o)}$  measured at 440 nm. TAS of (c)  $\text{STO:RS(NaCl)}$  and (d)  $\text{STO:RS(w/o)}$ . Theoretical calculated work functions of (e) {100} and (f) {110} facets of  $\text{STO:RS(NaCl)}$ .

PL and TAS analyses revealed enhanced charge separation in faceted  $\text{STO:RS(NaCl)}$ . Steady-state PL spectra exhibited broad emission bands ranging from 400 to 650 nm, with a peak at 440 nm (Fig. S12a, b), originating from the recombination of photogenerated carriers. Based on the time-resolved photoluminescence (TRPL) decay spectra and fitting results (Fig. 3a, b and Table S3),  $\text{STO:RS(NaCl)}$  exhibited a shorter average carrier lifetime ( $\tau_{AV} = 0.89$  ns vs. 1.16 ns for  $\text{STO:RS(w/o)}$ ), indicating that the faceted material exhibited enhanced non-radiative charge extraction compared to radiative recombination pathways.<sup>24</sup> TAS revealed significant differences in trap-state dynamics (Fig. 3c, d).  $\text{STO:RS(NaCl)}$  showed 56% weaker defect absorption ( $\Delta A = 0.8 \times 10^{-3}$  vs.  $1.8 \times 10^{-3}$  for  $\text{STO:RS(w/o)}$ ) at 650 nm, attributed to  $\text{Rh}^{4+}$ -related traps.<sup>25</sup> Cocatalyst modification further reduced the defect-induced absorption (Fig. S12c, d). Specifically, the residual trapping signal was attenuated by 50% upon Pt and CoOOH modified  $\text{STO:RS(NaCl)}$ . The collective evidence confirms anisotropic facets direct carriers to prefer separation transfer rather than

being trapped in defect states. Surface photovoltage (SPV) spectroscopy (Fig. S13) provided direct evidence about the surface charge accumulation.<sup>26,27</sup> It was found that  $\text{STO:RS(NaCl)}$  exhibited a sixfold stronger SPV signal than  $\text{STO:RS(w/o)}$ . Moreover, Pt/CoOOH loading further enhanced SPV (Fig. S13b), confirming that spatial separation of photogenerated charges allowed for faster and more efficient charge transfer to the material's surface and that the loading of cocatalysts can further enhance this effect. DFT simulations (Fig. 3e, f) revealed that the work functions of the {100} and {110} facets were 3.15 eV and 5.66 eV, respectively. The higher work function of {110} induced more pronounced surface band bending compared to {100}, generating a stronger built-in electric field in its space charge region that drove holes to accumulate on {110} and electrons on {100} (Fig. S14).<sup>28</sup> The resulting spatial charge separation creates distinct redox environments: hole-rich {110} favors oxidation (forming metal oxides), while electron-rich {100} favors reduction (forming metals).

The photocatalytic hydrogen evolution reaction (HER) is a crucial process where charge separation is mostly identified as the rate-limiting step.<sup>2</sup> In the case of  $\text{STO:RS(NaCl)}$ , Pt was used as HER cocatalyst and methanol as the sacrificial reagent. Photodeposited Pt on electron-rich {100} facet achieved twice the HER activity ( $3.1$  vs.  $1.7 \mu\text{mol}\cdot\text{h}^{-1}$ ) compared to randomly distributed Pt via impregnation (Fig. S15). CoOOH oxidation cocatalyst was photodeposited on {110} facet to synergistically enhance hole extraction. Loading dual-cocatalysts (0.50 wt% Pt and 0.75 wt% CoOOH) significantly boosted HER activity by 2.7-fold compared to single-cocatalyst (0.50 wt% Pt) systems (Fig. 4a). Based on Fig. S16 validation, optimal cocatalyst loading showed a volcano-shaped activity trend. With 0.5 wt% Pt fixed, activity peaked at 0.75 wt% CoOOH for  $\text{STO:RS(NaCl)}$ . The same trend occurred reciprocally (fixed 0.75 wt% CoOOH, varying Pt). This indicates moderate loading enhances charge extraction and reaction sites, while excess cocatalysts block light and hinder activity.

Pristine  $\text{STO:RS(NaCl)}$  and  $\text{STO:RS(w/o)}$  exhibited negligible HER activity (Fig. 4b), but after photodeposition of dual cocatalysts (0.50 wt% Pt and 0.75 wt% CoOOH),  $\text{STO:RS(NaCl)}$  achieved three times higher HER rate ( $9.2$  vs.  $2.9 \mu\text{mol}\cdot\text{h}^{-1}$ ) than  $\text{STO:RS(w/o)}$ , despite identical Rh/Sb doping (ICP-OES) and light absorption (UV-vis DRS). This superior performance of  $\text{STO:RS(NaCl)}$  was attributed to the directional migration of photogenerated electrons and holes, which effectively improved the carrier separation efficiency. In the linear sweep voltammetry (LSV) test,  $\text{STO:RS(NaCl)}$  exhibited a higher photocurrent compared to  $\text{STO:RS(w/o)}$  (Fig. S17a). After spatially selective photodeposition, Pt-CoOOH/ $\text{STO:RS(NaCl)}$  exhibited the highest photocurrent response, suggesting that the loading of dual-cocatalysts could extract carriers more effectively (Fig. S17b). In addition, the smaller Nyquist curve radius in the electrochemical impedance spectroscopy (EIS) test for  $\text{STO:RS(NaCl)}$  demonstrated lower charge transfer resistance compared to  $\text{STO:RS(w/o)}$  (Fig. S17c). HER stability was confirmed through cyclic tests (Fig. 4c) with consistent performance, and the post-reaction STEM analysis (Fig. S18) showed that the  $\text{STO:RS(NaCl)}$  retained its single-crystalline





structure, while the Pt cocatalyst maintained intimate interfacial contact with STO. Wavelength dependence experiments (Fig. 4d) demonstrated that photocatalytic hydrogen production was directly linked to light absorption.

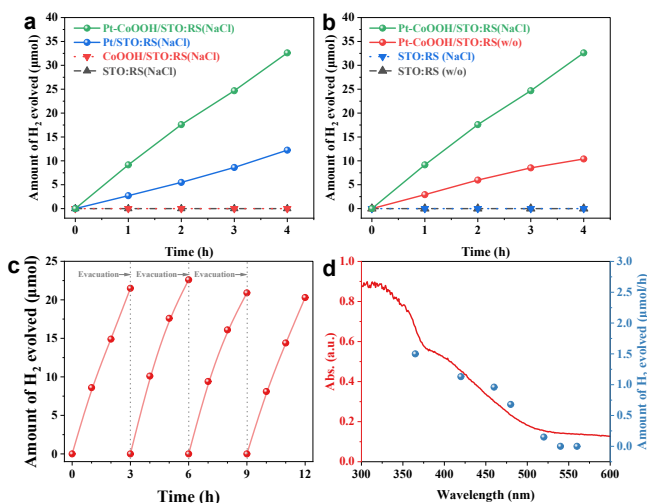


**Fig. 4** (a) HER on STO:RS(NaCl) loaded with different cocatalysts via photodeposition. (b) HER on STO:RS(NaCl) and STO:RS(w/o) with or without Pt/CoOOH loaded. (c) Curves of multiple cycles of activity as a function of reaction time. (d) Wavelength dependence of HER.

In summary, we demonstrated a visible-light-active SrTiO<sub>3</sub> photocatalyst (STO:RS(NaCl)) with facet-dependent charge separation, synthesized via Rh/Sb co-doping and NaCl flux treatment. Systematic characterization (photodeposition, PL, TAS, SPV) confirmed electrons and holes migrate to {100} and {110} facets, respectively, and facilitate the improvement of carrier separation efficiency, which was driven by facet-specific work function differences. The photocatalytic hydrogen evolution of STO:RS(NaCl) is three times higher than that of STO:RS(w/o). The work established a dual strategy – doping for visible absorption and facet engineering for charge rectification – providing a blueprint for designing efficient solar-driven semiconductors.

This work was supported by the National Natural Science Foundation of China (21925206, 22409022), Dalian Supports High-level Talent Innovation and Entrepreneurship Projects (2020RD06), and Liaoning Revitalization Talents Program (XLYC1807241).

## Conflicts of interest

There are no conflicts to declare.

## Data availability

The data supporting this article have been included as part of the ESI.†

## Notes and references

- X. Tao, Y. Zhao, S. Wang, C. Li and R. Li, *Chem. Soc. Rev.*, 2022, **51**, 3561–3608. DOI: 10.1039/D5CC04308E
- Y. Xu, A. Li, T. Yao, C. Ma, X. Zhang, J. H. Shah and H. Han, *ChemSusChem*, 2017, **10**, 4277–4305.
- X. Guan, S. Zong and S. Shen, *Nano Res.*, 2022, **15**, 10171–10184.
- J. Yang, D. Wang, H. Han and C. Li, *Acc. Chem. Res.*, 2013, **46**, 1900–1909.
- S. Wang, G. Liu and L. Wang, *Chem. Rev.*, 2019, **119**, 5192–5247.
- H. G. Yang, C. H. Sun, S. Z. Qiao, J. Zou, G. Liu, S. C. Smith, H. M. Cheng and G. Q. Lu, *Nature*, 2008, **453**, 638–641.
- Y. Deng, H. Zhou, Y. Zhao, B. Yang, M. Shi, X. Tao, S. Yang, R. Li and C. Li, *Small*, 2022, **18**, 2103245.
- J. Zhang, K. Liu, B. Zhang, J. Zhang, M. Liu, Y. Xu, K. Shi, H. Wang, Z. Zhang, P. Zhou and G. Ma, *J. Am. Chem. Soc.*, 2024, **146**, 4068–4077.
- R. Li, H. Han, F. Zhang, D. Wang and C. Li, *Energy Environ. Sci.*, 2014, **7**, 1369–1376.
- T. Takata, J. Jiang, Y. Sakata, M. Nakabayashi, N. Shibata, V. Nandal, K. Seki, T. Hisatomi and K. Domen, *Nature*, 2020, **581**, 411–414.
- K. Domen, S. Naito, M. Soma, T. Onishi and K. Tamaru, *J. Chem. Soc., Chem. Commun.*, 1980, DOI: 10.1039/C39800000543, 543–544.
- T. Takata and K. Domen, *J. Phys. Chem. C*, 2009, **113**, 19386–19388.
- L. Mu, Y. Zhao, A. Li, S. Wang, Z. Wang, J. Yang, Y. Wang, T. Liu, R. Chen, J. Zhu, F. Fan, R. Li and C. Li, *Energy & Environmental Science*, 2016, **9**, 2463–2469.
- Y. Zhang, X. Wu, Z.-H. Wang, Y. Peng, Y. Liu, S. Yang, C. Sun, X. Xu, X. Zhang, J. Kang, S.-H. Wei, P. F. Liu, S. Dai and H. G. Yang, *J. Am. Chem. Soc.*, 2024, **146**, 6618–6627.
- H. Nishiyama, T. Yamada, M. Nakabayashi, Y. Maehara, M. Yamaguchi, Y. Kuromiya, Y. Nagatsuma, H. Tokudome, S. Akiyama, T. Watanabe, R. Narushima, S. Okunaka, N. Shibata, T. Takata, T. Hisatomi and K. Domen, *Nature*, 2021, **598**, 304–307.
- Z. Pan, J. J. M. Vequizo, H. Yoshida, J. Li, X. Zheng, C. Chu, Q. Wang, M. Cai, S. Sun, K. Katayama, A. Yamakata and K. Domen, *Angew. Chem. Int. Ed.*, 2025, **64**, e202414628.
- H. Kato, M. Kobayashi, M. Hara and M. Kakihana, *Catal. Sci. Technol.*, 2013, **3**, 1733–1738.
- A. R. Denton and N. W. Ashcroft, *Phys. Rev. A*, 1991, **43**, 3161–3164.
- R. Shannon, *Acta Crystallogr. A*, 1976, **32**, 751–767.
- R. Niishiro, S. Tanaka and A. Kudo, *Appl. Catal. B Environ. Energy*, 2014, **150–151**, 187–196.
- S. Assavachin, C. Xiao, K. Becker and F. E. Osterloh, *Energy Environ. Sci.*, 2024, **17**, 3493–3502.
- Y. Matsumoto, *J. Solid State Chem.*, 1996, **126**, 227–234.
- H. Lyu, T. Hisatomi, Y. Goto, M. Yoshida, T. Higashi, M. Katayama, T. Takata, T. Minegishi, H. Nishiyama, T. Yamada, Y. Sakata, K. Asakura and K. Domen, *Chemical Science*, 2019, **10**, 3196–3201.
- Y. Deng, Q. Li, P. Wang, F. Sun, C. Li and R. Li, *Catal. Sci. Technol.*, 2024, **14**, 4228–4235.
- J. J. M. Vequizo, S. Nishioka, J. Hyodo, Y. Yamazaki, K. Maeda and A. Yamakata, *J. Mater. Chem. A*, 2019, **7**, 26139–26146.
- Y. Li, Z. Liu, J. Li, M. Ruan and Z. Guo, *J. Mater. Chem. A*, 2020, **8**, 6256–6267.
- Q. Wang, X. Zhan, C. Fan, X. Yang, B. Li, H. Liu, Y. Wu, K. Zhang and P. Tang, *J. Mater. Chem. A*, 2024, **12**, 33290–33300.
- S.-C. Chan, Y.-L. Cheng, B. K. Chang and C.-W. Hong, *RSC Adv.*, 2021, **11**, 18500–18508.



## Data Availability Statement

### Facet-dependent spatial charge separation in metals-doped SrTiO<sub>3</sub> photocatalyst with visible light utilization

Xueshang Xin,<sup>ab</sup> Shiwen Du,<sup>a</sup> Yejun Xiao,<sup>c</sup> Hai Zou,<sup>ab</sup> Yunfeng Bao,<sup>a</sup> Yu Qi,<sup>a</sup> Shengye Jin,<sup>c</sup> Zhaochi Feng,<sup>a</sup> and Fuxiang Zhang<sup>\*a</sup>

<sup>a</sup> State Key Laboratory of Catalysis, Dalian National Laboratory for Clean Energy

Dalian Institute of Chemical Physics

Chinese Academy of Sciences

Dalian, 116023, China

E-mail: fxzhang@dicp.ac.cn

<sup>b</sup> Center of Materials Science and Optoelectronics Engineering

University of Chinese Academy of Sciences

Beijing, 100049, China

<sup>c</sup> State Key Laboratory of Molecular Reaction Dynamics and Dynamics Research Center for Energy and Environmental Materials

Dalian Institute of Chemical Physics

Chinese Academy of Sciences

Dalian, 116023, China

The data supporting this article have been included as part of the Supplementary Information.

